CrystEngComm

Accepted Manuscript

ROYAL SOCIETY OF CHEMISTRY

www.rsc.org/crystengcomm

Cite this: DOI: 10.1039/c0xx00000x

www.rsc.org/xxxxxx

ARTICLE TYPE

Phase controlled synthesis of SnSe and $SnSe_2$ hierarchical nanostructures made of single crystalline ultrathin nanosheets†

Parthiban Ramasamy, Palanisamy Manivasakan, and Jinkwon Kim*

Received (in XXX, XXX) Xth XXXXXXXXX 20XX, Accepted Xth XXXXXXXXX 20XX

DOI: 10.1039/b000000x

The electronic and optoelectronic properties of tin selenide nanostructures are of great interest for application in energy conversion and storage devices. Despite the great progress has been achieved in nanoparticle synthesis, controlling the crystal phase in tin selenide nanostructures remains a challenge. In this article, we present a simple solvothermal approach for the phase controlled synthesis of SnSe and $SnSe_2$ hierarchical nanostructures (HNs) for the first time. SnSe HNs has been prepared by reacting $SnCl_4$ and SeO_2 under solvothermal condition using oleylamine as solvent. By adding calculated amount of 1-dodecanethiol (1-DDT) to the reaction mixture the crystal phase can be tuned from SnSe to $SnSe_2$. The obtained HNs were comprised of single crystalline thin nanosheets with thickness in the range of 7-12 nm. A possible mechanism has been proposed for the phase controlled synthesis of tin selenides. The obtained SnSe and $SnSe_2$ HNs showed good electrocatalytic activity in the redox reaction of the I^-/I_3^- shuttle. Dye sensitized solar cells (DSSC) employing SnSe and $SnSe_2$ HNs as counter electrodes showed photovoltaic performances similar to the device made with conventional platinum (Pt) counter electrode.

1. Introduction

Over the past two decades, nanostructures of semiconductor chalcogenides have been extensively studied, because of their potential application in optoelectronic devices.[1-3] In the case of IV-VI chalcogenides, most of the studies have focused on PbS and PbSe nanocrystals since their band gap can be tuned across the infrared and visible spectrum by varying the nanocrystals size.[4-6] On the other hand, relatively less attention has been paid on the synthesis and studies of tin based chalcogenides such as SnS, SnSe and SnTe. Amongst tin chalcogenides, tin selenides are an important narrow band gap IV-VI semiconductors having a wide range of applications such as solar cells, supercapacitors, infrared optoelectronic devices, memory switching devices and anode materials for lithium-ion batteries.[7-12] Tin selenide materials exist in two stoichiometric phases in the form of tin monoselenide (SnSe) and tin diselenide ($SnSe_2$). SnSe is a p-type semiconductor with narrow band gap (~0.90 eV indirect and ~1.30 eV direct), adopts features of an orthorhombic layered structure that facilitates two-dimensional growth.[13] Whereas, $SnSe_2$ is an n-type semiconductor which has the layered CdI_2-type structure, in which each layer of Sn atoms is sandwiched between two layers of hexagonally close-packed Se atoms, and the adjacent selenium layers are connected by the weak van der Waals interaction.

Recently, several research groups have reported the colloidal synthesis of tin selenide nanomaterials of diverse size and shapes such as nanoparticles, nanowires, nanosheets, and nanocolumns.[14-18] Most of the synthetic methods involve the use of trioctylphosphine selenide (TOPSe) as selenium source. However, phosphines are expensive, toxic and highly sensitive to air. In addition, controlling the composition or phase of the final tin selenide has been a big task, since the Sn^{2+} in precursor is often oxidised to Sn^{4+} and resulted in final composition of $SnSe_2$ instead of SnSe.[12] *Jang et al.* proposed a solution to control the phase by synthesizing single source precursor containing Sn and Se atoms and decompose in oleylamine.[18] Although this method was successful, the synthesis of precursor is more laborious and needs dry reaction conditions. Besides the phase controlled synthesis, shape controlled nanomaterials synthesis is an another important aspect due to the fact that many physical properties of nanomaterials are highly shape dependant. In recent years, hierarchical nanostructures consist of interconnected small nanoscale building blocks such as nanorods or nanosheets have received great research interest. Hierarchical nanostructures can provide high surface areas and good particle stabilities as well as better carrier transport capability.[19,20] Hierarchical nanostructures have shown improved performance in various devices. In particular, when used in counter electrodes of DSSC, hierarchical nanostructures exhibited higher efficiencies than the nanoparticle counter electrodes.[21-23] Thus, developing simple and facile synthetic approaches that yield tin selenide nanostructures with precise control over the chemical composition and shape is highly desirable for both fundamental studies and practical applications.

Here, we report a facile solution method for the phase-controlled synthesis of 3D hierarchical tin selenide nanostructures that is assembled by thin single-crystal nanosheets. The synthetic method involves the solvothermal reaction between $SnCl_4 \cdot 5H_2O$ and SeO_2 in oleylamine using 1-dodecanethiol as surfactant. The salient features of our synthetic method are as follows: (1) Toxic, expensive and air-sensitive precursors such as bis-

(trimethylsilyl)selenide and TOPSe have been replaced with inexpensive and air-stable SeO_2. (2) phase pure SnSe or $SnSe_2$ hierarchical nanostructures can be synthesized by controlling the reaction parameters. (3) nanosheets thickness in $SnSe_2$ hierarchical nanostructures can be tuned by using selective surfactants . To the best of our knowledge this the first report on phase controlled synthesis of 3D hierarchical tin selenide nanostructures. The possible application of tin selenides as prominent alternative to platinum free counter electrode in DSSC has been demonstrated for the first time. DSSC device with $SnSe_2$ HNs counter electrode exhibits a promising power conversion efficiency of 5.60% comparable to that of the device using Pt counter electrode (5.74%).

2. Experimental

2.1. Synthesis of SnSe hierarchical nanostructures

In a typical synthesis, 0.2 mmol of $SnCl_4 \cdot 5H_2O$, and 0.2 mmol of SeO_2 were added to 17 mL of oleylamine in a clean 50 mL flask at room temperature followed by heating at 70 °C for 30 min to get a transparent solution. Then, the obtained transparent solution was transferred to 25 mL Teflon lined autoclave and heated to 180 °C for 24 h in an electric oven. When the reaction was finished, the autoclave was cooled down to room temperature, the supernatant was decanted, and the resulting precipitate was washed with toluene and ethanol mixture (1:2) three times, dried under vacuum.

2.2. Synthesis of $SnSe_2$ hierarchical nanostructures

200 µL of 1-dodecanethiol was added to 17 mL oleylamine followed by the addition of 0.2 mmol of $SnCl_4 \cdot 5H_2O$, and 0.2 mmol of SeO_2. The mixture was heated at 70 °C for 30 min and clear yellow colour solution was obtained. The obtained mixture was transferred to 25 mL Teflon lined autoclave and heated to 180 °C for 36 h in an electric oven. When the reaction was finished, the autoclave was cooled down to room temperature, the supernatant was decanted, and the resulting precipitate was washed with toluene and ethanol mixture (1:2) three times, dried under vacuum.

2.3. Fabrication of CEs and DSSCs

The reference Pt CE was prepared by deposition of 50 µL H_2PtCl_6 isopropanol solution (3 mM) on the FTO glass followed by 500 °C heat treatment for 30 min in air. SnSe and $SnSe_2$ CEs were prepared by deposition of 50 µL toluene dispersions (10 mg/mL) on the FTO glass followed by 500 °C heat treatment for 30 min in N_2 atmosphere.

TiO_2 paste was prepared according to reported literature procedures.[24] TiO_2 paste was coated on a conducting glass with F:SnO_2 film (FTO,7 Ω sq^{-1}, Aldrich) using a doctor-blade printing technique. After printing, the electrode was dried at 70 °C and then was sintered at 450 °C for 30 min in air. After sintering at 450 °C, the TiO_2 films were treated with 40 mM $TiCl_4$ at 70 °C for 30 min, rinsed with water and ethanol and sintered at 450 °C for 30 min. At 80 °C in the cooling, the TiO_2 electrode was immersed into dye solution (N719, Solaronix, 0.5 mM in ethanol), and kept at the room temperature for 21 h. The dye-adsorbed TiO_2 electrode and counter electrode were stacked and sealed with a sealant (Surlyn, 60 mm-thick, Meltonix) at 100 °C for 15s. The electrolyte solution of composition with 1.0 M 1,3-dimethylimidazolium iodide, 0.03 M I_2, 0.1 M guanidinium thiocyanate, 0.5 M tert-butylpyridine, 0.05 M LiI in acetonitrile and valeronitrile (85/15, v/v) was injected into the cell through a hole and end sealed.

2.4. Characterization

The products were characterized by X-ray diffraction (XRD, Rigaku Miniflex II), field emission scanning electron microscopy (FESEM, Hitachi S-4800 UHR), transmission electron microscopy (TEM, JEOL JEM-2100F), and X-ray photoelectron spectroscopy (XPS, Multilab ESCA 2000). Diffuse reflectance spectra were recorded on a UV-3600 shimadzu UV-vis-NIR spectrophotometer. The Brunauer–Emmett–Teller (BET) surface area and pore size distribution were determined using an ASAP-2420 accelerated surface area and porosimetry system (Micromeritics, USA). Cyclic voltammetry (CV) was conducted in a three-electrode system in an acetonitrile solution of 0.1 M $LiClO_4$, 10 mM LiI, and 1 mM I_2 at a scan rate of 20 mV s^{-1} by using a BAS100 B/W electrochemical analyzer. Platinum served as a CE and the Ag/Ag^+ couple was used as a reference electrode. Solar energy conversion efficiency was measured using solar simulator (Oriel Sol 3A Solar Simulator, 94063A, Newport Stratford Inc.) under a simulated standard solar light, *i.e.,* 100 mW cm^{-2}; AM1.5G checked with an NREL-calibrated Si-solar cell.

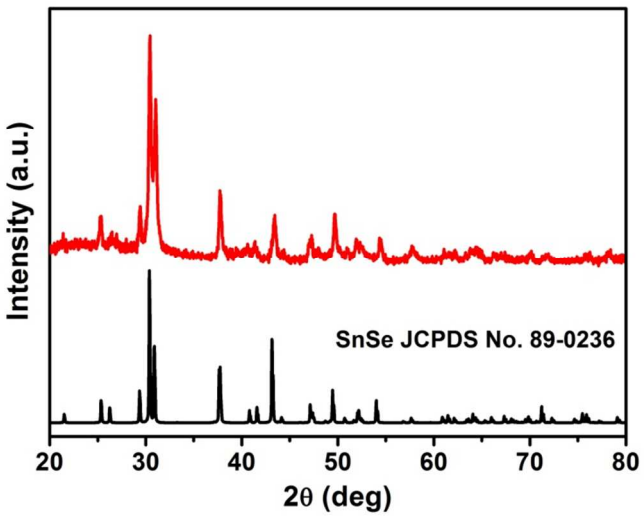

Fig. 1 XRD pattern of SnSe nanostructures.

3. Results and Discussions

3.1. Synthesis of SnSe hierarchical nanostructures

The crystallinity and crystal phases of the SnSe HNs were characterized by X-ray diffraction studies. Fig. 1, shows the XRD pattern of the as prepared SnSe HNs. All the observed diffraction peaks can be indexed to orthorhombic-phase SnSe (JCPDS No. 89-0236, *Pnma*). No other additional phases were observed, which further confirms the purity of the SnSe nanostructures. The oxidation states of Sn and Se in SnSe HNs were investigated by XPS. The Sn $3d_{3/2}$ and Sn $3d_{5/2}$ orbital peaks were observed at 494.1 and 485.7 eV, respectively, and Se 3d peak was located at 53.5 eV (Fig. S1, ESI†). This confirms the +2 and -2 valence states for Sn and Se in SnSe HNs.[18] The purity of the SnSe HNs was further confirmed by EDS analysis (Fig. S2, ESI†). The observed Sn/Se ratio of 1:1, is in accordance with the stoichiometry of SnSe.

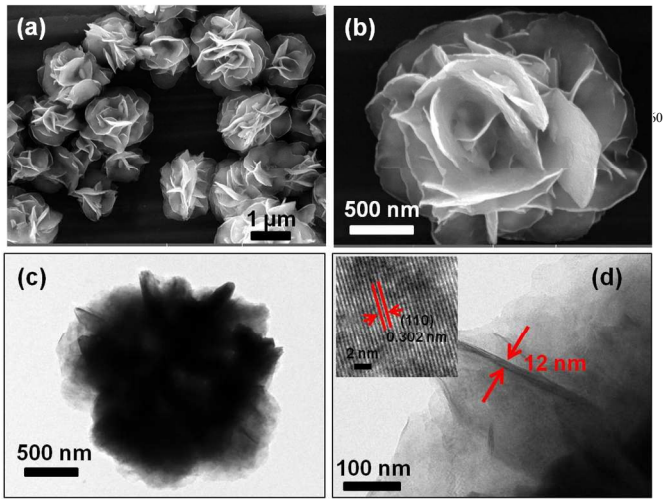

Fig. 2 (a,b) SEM images, and (c,d) TEM images of SnSe hierarchical nanostructures. The inset is the HRTEM image.

The morphologies of the SnSe were characterized using field-emission scanning electron microscope (FESEM) and transmission electron microscope (TEM). As shown in Fig. 2a,b, the prepared SnSe possess hierarchical flower-shaped morphologies. The SnSe hierarchical nanostructures were nearly uniform in size with the average diameter of 1.5 - 2 μm. Interestingly, it was observed that the flower-like nanostructures are comprised of individual thin nanosheets as "petals" connected to a central core. TEM image in Fig. 2c is in full consistency with the FESEM observations in terms of shape and size of the nanostructures. The thickness of an individual nanosheet was found to be 12 nm (Fig. 2d). The HRTEM analysis (inset in Fig. 2d) shows clear lattice fringes and the calculated interplanar distance between the two adjacent lattice planes was 0.302 nm, corresponding to the (110) plane of the orthorhombic phase SnSe.

In order to study the formation process of SnSe hierarchical nanostructures, time dependent experiments were carried out. XRD patterns of the SnSe nanostructures at different reaction time are shown in Fig. S3 (ESI†). All the XRD patterns are well matched with orthorhombic phase SnSe. Fig. 3 shows the SEM images of SnSe HNs synthesized at different reaction times. When the reaction time was less than 12 h, no solid products were obtained and the reaction mixture was turbid yellow colour. After 12 h reaction time, sheet-like SnSe forms as a general morphology due to its layered structure. The formation of nanosheets can be explained by nanoparticles aggregation mechanism which is well studied.[16] In the earlier stage of the reaction, individual nanoparticles seeds are formed and as the reaction time increases these nanoparticles started to coalesce and form the initial nanosheets structure. Besides acting as a reducing agent, oleylamine could coordinate to the Sn^{2+} ions to form complexes in solution, which decreases the free Sn^{2+} concentration in solution and results in the slow generation of SnSe nanoparticle seeds. These nanoparticle seeds are assemble on the surface of the preformed nanosheets and coalesced to increase the number of nanosheets layer. When the reaction time was increased to 15 h, flower-like morphology begins to emerge, as the nanosheet "petals" protrude from the nanosheets assemblies. With the increasing reaction time, the Ostwald ripening process occurs, the crystal core with a higher density dissolves and transferred to outer nanosheets with a lower density by a dissolution-recrystallization process, and these nanosheets continue to grow in size to become final flower-like petals.

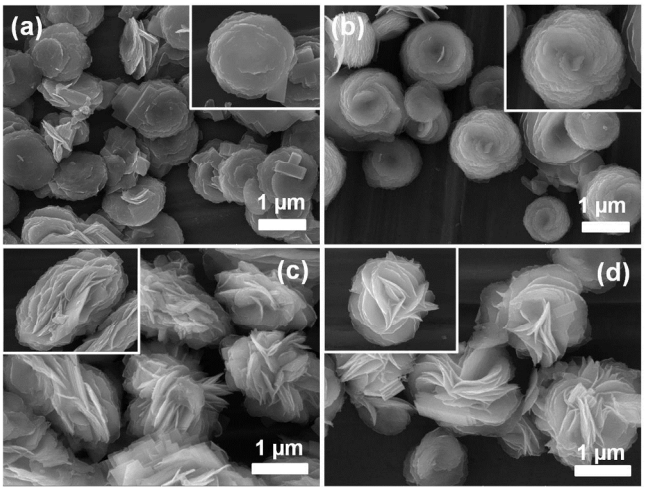

Fig. 3 SEM images showing the growth process of the SnSe hierarchical nanostructures with different reaction times. (a) 12 h, (b) 15 h, (c) 18 h, and (d) 21 h. Inset show the single SnSe HNs.

3.2. Synthesis of $SnSe_2$ hierarchical nanostructures

$SnSe_2$ HNs can be readily obtained by adding certain amount of 1-dodecanethiol to the reaction system used for SnSe HNs. Fig. 4 shows the XRD pattern of the products obtained with different amount of 1-DDT at 180 ºC for 36 h. When 50 or 100 μL of 1-DDT was added, the obtained products were mixture of orthorhombic SnSe and hexagonal $SnSe_2$. Phase pure hexagonal $SnSe_2$ HNS were obtained when 200 μL of 1-DDT was added to the reaction mixture. In addition, XPS spectra (Fig. S4, ESI†) showed Sn $3d_{3/2}$ and $3d_{5/2}$ orbital peaks at 495.8 and 487.5 eV, respectively, and Se 3d orbital peak at 54.9 eV, which further confirms the formation of pure hexagonal $SnSe_2$.[17] The chemical

stoichiometry of the obtained $SnSe_2$ HNs was investigated by EDS analysis. EDS spectra in Fig. S5 (ESI†) shows the measured Sn/Se ratio of 1:2.1 which agrees well with the stoichiometry of $SnSe_2$.

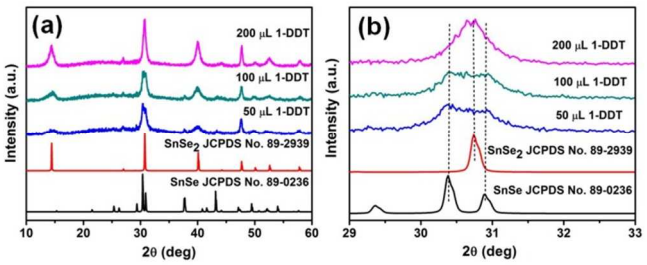

Fig. 4 (a, b) XRD patterns of the products obtained with different amounts of 1-DDT.

As can be seen from the FESEM images shown in Fig. 5, both the mixed phase SnSe-$SnSe_2$ and pure $SnSe_2$ have hierarchical flower-like morphologies. This is similar to the results obtained for SnSe nanostructures. The average size of the $SnSe_2$ HNs were 3-4 μm (Fig. 5c,d), which is two times larger than the SnSe nanostructures. It is interesting to observe that the added 1-DDT only influenced the crystal phase of the tin selenides and did not have any significant effect on the morphologies of the products.

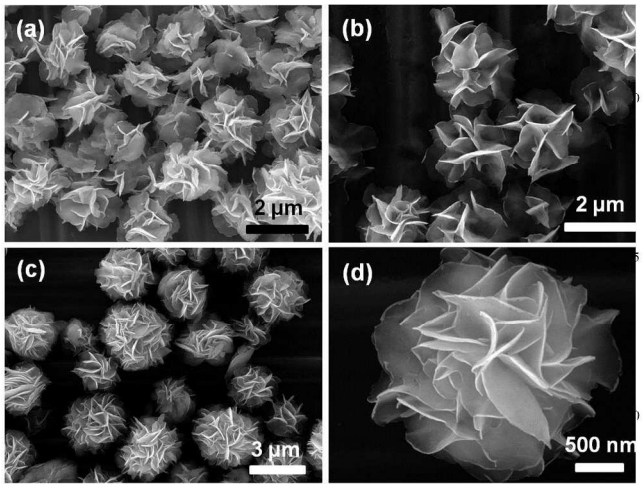

Fig. 5 SEM images the products obtained with different amounts of 1-DDT (a) 50, (b) 100, and (c,d) 200 μL.

Fig. 6 shows the TEM characterization of the $SnSe_2$ hierarchical nanostructures. Flower-like morphology of $SnSe_2$ nanostructures can be clearly seen in Fig. 6a, and the thickness of the constituting nanosheets were about 7-10 nm (Fig. 6b and Fig. S6 (ESI†)). Fig. 6c shows the TEM image of a single nanosheet. The nanosheet is hexagonal in shape and diameter about 1 μm. In HRTEM analysis on the single nanosheets (Fig. 6d), the (100) set of planes with 0.330 nm interplanar distance were predominantly observed. In addition, the selected area electron diffraction pattern (SAED) shows the spot pattern consistent with the single crystal nature of the nanosheet (inset in Fig. 6d).

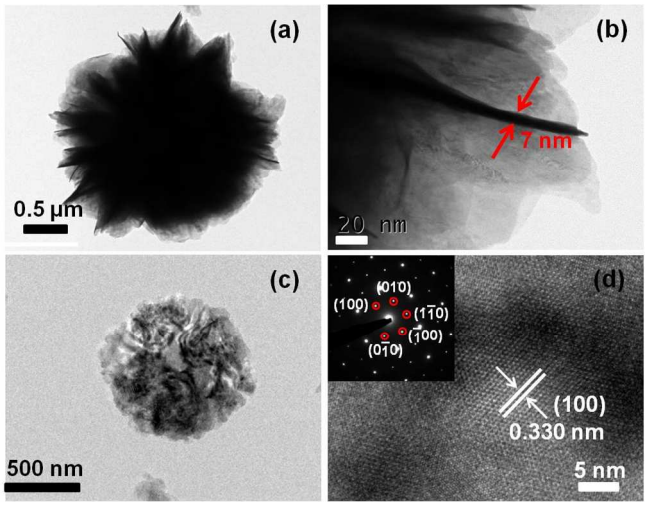

Fig. 6 (a,b) TEM images of $SnSe_2$ hierarchical nanostructures. (c) TEM image of single $SnSe_2$ nanosheet. (d) HRTEM and SAED pattern of $SnSe_2$ nanosheet.

On the basis of the above experimental results, a possible mechanism for the formation of phase controlled tin selenides HNs can be proposed. Fig. 7 shows the schematic for the formation of SnSe and $SnSe_2$ HNs. Before transferring to autoclave, the reaction mixture was heated at 70 °C for 30 min to completely dissolve $SnCl_4$ and SeO_2 in oleylamine. In the absence of 1-DDT, added Sn^{4+} ions were reduced to Sn^{2+} by oleylamine which further reacts with Se^{2-} to produce SnSe HNs. On the other hand, in the presence of 1-DDT, Sn^{4+} first reacts with 1-DDT to form Sn^{4+}-dodecanethiolate complex. This stabilizes the Sn^{4+} ions in oleylamine medium, which later react with Se^{2-} to form $SnSe_2$ HNS. Phase pure $SnSe_2$ HNs were obtained only when 200 μL of DDT was used. This gives a mole ratio of nearly 1:6 between Sn^{4+} and 1-DDT, which means for each Sn^{4+} ion there are six 1-DDT molecules available to form Sn^{4+}-dodecanethiolate complex. Since dodecanethiolate is a monodentate ligand, minimum four molecules of 1-DDT are required to effectively stabilize one Sn^{4+} ion. Hence, 200 μL of 1-DDT is sufficiently enough to stabilize Sn^{4+} ions in the reaction mixture and formed pure $SnSe_2$ HNs. On the other hand, when 50 or 100 μL of DDT were used, the mole ratio between Sn^{4+} and 1-DDT decreased to 1:1.5 and 1:3, respectively. Sn^{4+} ions cannot be completely stabilized with these concentrations of 1-DDT and resulted in mixed phase of SnSe and $SnSe_2$ (Fig. 4). Furthermore, with 1-DDT the reaction mixture changed from colourless to bright yellow colour after stirring at 70 °C for 30 min. This further confirms the formation of Sn^{4+}-dodecanethiolate complex. $SnSe_2$ HNs were formed only after 36 h, which is relatively longer reaction time than that of SnSe HNs (24 h). This can be attributed to the stability of Sn^{4+}-dodecanethiolate complex which slowed down the formation of $SnSe_2$ nuclei. In order to further support this mechanism, we carried out similar experiments with oleic acid instead of 1-DDT. Different amounts of oleic acid (100, 300 and 500 μL) were added to the reaction

mixture and the reaction was performed at 180 °C for 36 h. Oleic acid can react with Sn^{4+} ion and form Sn-oleate complex. XRD patterns in Fig. S7 (ESI†) show that pure $SnSe_2$ phase was obtained only when certain amount of oleic acid is presented in the reaction medium. Fig. S8 (ESI†) shows the SEM images of $SnSe_2$ HNs synthesized with oleic acid. The morphology of the HNs are slightly different from those obtained with 1-DDT. The constituting nanosheets have an average thickness of 20 nm.

3.3. Optical properties of SnSe and $SnSe_2$ HNs

Diffuse reflectance data were obtained to study the optical properties of SnSe and $SnSe_2$ HNs. Samples were prepared by drop-casting a concentrated toluene dispersions of tin selenides on glass substrates. Onset absorption was found to be near 1200 nm for SnSe HNs and 1000 nm for $SnSe_2$ HNs, respectively (Fig. S9 and S10, ESI†). Kubelka-Munk transformations were performed to determine the indirect and direct bandgap values.[16] The indirect band gaps of the SnSe and $SnSe_2$ HNs were determined to be 1.01 and 1.28 eV, and the direct band gaps were 1.36 eV for SnSe and 1.42 eV for $SnSe_2$ HNs, respectively. In addition, We have measured the optical properties of SnSe nanostructures as a function of reaction time. The diffuse reflectance spectra is provided in Fig. S11 (ESI†) and the calculated direct and indirect bandgap values are listed in Table S1 (ESI†). The direct bandgap values are decreased with increasing reaction time, whereas the indirect bandgap values are increased with increasing reaction time. We have also measured the optical properties of SnSe/$SnSe_2$ composite nanostructures synthesized using 100 µL 1-DDT. The indirect and direct bandgap values were determined to be 0.97 and 1.29 eV, respectively (Fig S12, ESI†).

3.4. Photovoltaic application of SnSe and $SnSe_2$ HNs

The photovoltaic potentials of SnSe and $SnSe_2$ HNs were assessed by employing them as counter electrodes in DSSCs. SnSe and $SnSe_2$ CEs were prepared by deposition of 50 µL toluene dispersions (10 mg/mL) on the FTO glass followed by 500 °C heat treatment for 30 min in N_2 atmosphere. The textural properties of the annealed SnSe and $SnSe_2$ HNs were obtained through N_2 adsorption–desorption isotherms and details of the data profiles are given in Fig. S13 and S14 (ESI†). The Brunauer–Emmett–Teller (BET) surface area of SnSe and $SnSe_2$ HNs were measured to be 3.9 and 5.2 m^2/g, respectively. These values are higher than the reported surface area for $SnSe_2$ nanostructures.[25] Both the HNs nanostructures possessed mesoporous nature with pore size distribution around 10-40 and 5-10 nm for SnSe and $SnSe_2$ HNs, respectively. The morphology of the annealed films was characterized using SEM analysis. As shown in Fig. S15 (ESI†), both the films were dense and uniform without any major cracks. No obvious change in the flower-like morphology was observed. This shows the structural stability of tin selenides at high temperatures. The thickness of the films were measured from the cross-sectional SEM images of the films. SnSe and $SnSe_2$ HNs films have an average thickness of 7.5 and 9.5 µm Fig. S16 (ESI†). We also characterized the films using XRD before and after annealing at 500 °C. The XRD patterns are shown in Fig. S17 and S18 (ESI†). No additional peaks or changes in the XRD pattern were observed after annealing at 500 °C. The electrocatalytic activity of the as prepared CEs was evaluated using cyclic voltammetry (CV) in a three-electrode system. Fig. 8a shows the CV curves for I^-/I_3^- redox couple on Pt, SnSe, and $SnSe_2$ CEs. For all the three electrodes, two pairs of redox peaks were observed in the cyclic voltammograms. The left redox peaks correspond to eqn (1) and the right redox peaks correspond to eqn (2). Both the SnSe and $SnSe_2$ CEs show similar redox peaks compared to Pt, indicating that tin selenides are effective in catalyzing the reduction of triiodide to iodide.

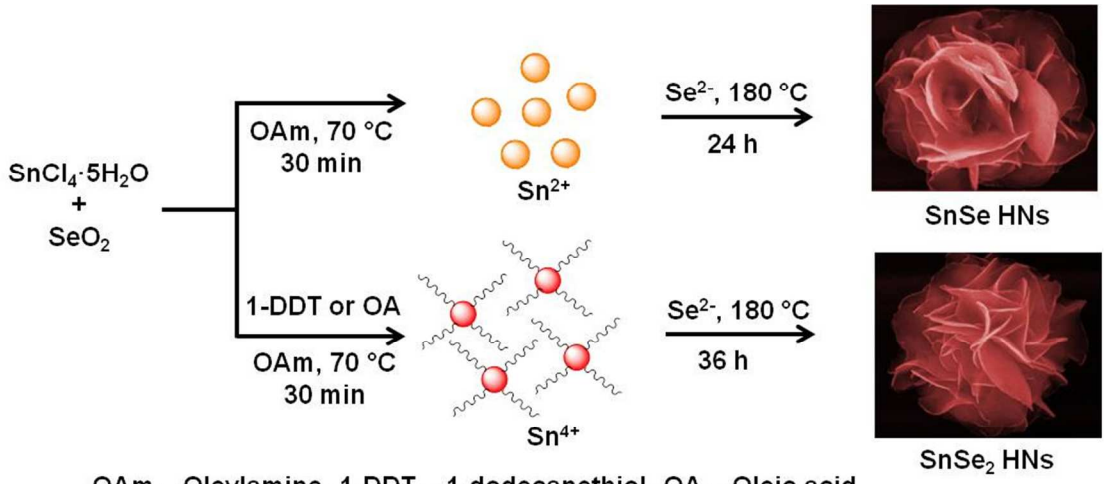

Fig. 7 Schematic for the phase controlled synthesis of tin selenides.

$$I_3^- + 2e^- \longleftrightarrow 3I^- \quad (1)$$

$$3I_2 + 2e^- \longleftrightarrow 2I_3^- \quad (2)$$

Figure 8b shows the current density-voltage (J–V) curves of N719-sensitized solar cells assembled with various CEs under a standard simulated AM 1.5 illumination of 100 mWcm^{-2}. The detailed photovoltaic parameters are summarized in Table 1. The DSSC with $SnSe_2$ CE yielded a power conversion efficiency (PCE) of 5.60% (short-circuit photocurrent density (J_{sc}) = 10.71 mA cm^{-2}, open-circuit photovoltage (V_{oc}) = 0.747 V, fill factor (FF) = 0.70), while the DSSC with SnSe CE produced a PCE of 5.52% (J_{sc} = 10.38 mA cm^{-2}, V_{oc} = 0.760 V, FF = 0.70). These result were comparable to the performance of the reference DSSC device using the conventional Pt CE with PCE of 5.74% (J_{sc} = 10.98 mA cm^{-2}, V_{oc} = 0.756 V, FF = 0.69). These results suggest that the synthesized SnSe and $SnSe_2$ HNs are promising candidates to replace the precious Pt metal as an efficient electrocatalyst in DSSCs.

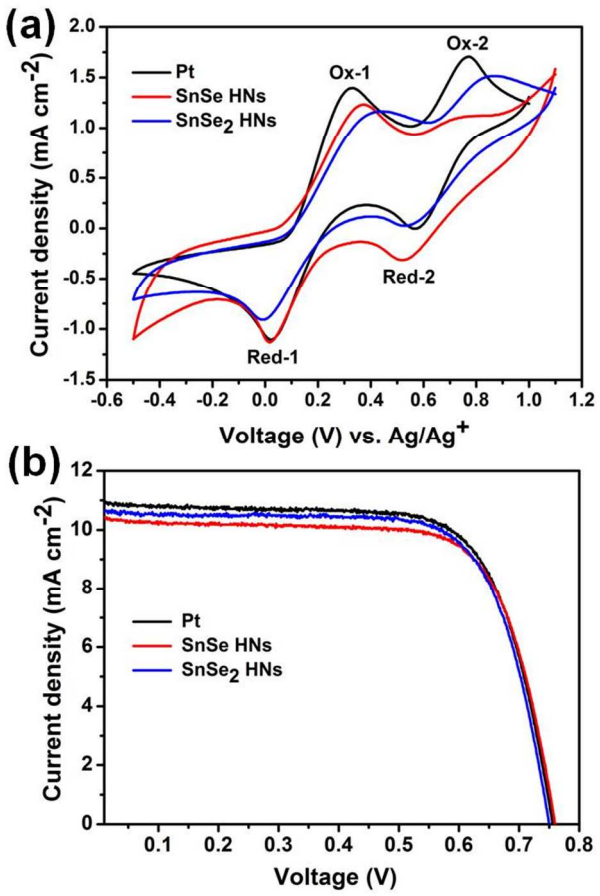

Fig. 8 (a) CV curves of iodide/triiodide redox species for Pt, SnSe, and $SnSe_2$ HNs electrodes, respectively. (b) J-V curves of DSSCs with different counter electrodes.

Table 1 Photovoltaic characteristics of DSSCs with different CEs

CEs	J_{sc}/mAcm^{-2}	V_{oc}/V	FF	η/%
Pt	10.98	0.756	0.69	5.74
SnSe HNs	10.38	0.760	0.70	5.52
$SnSe_2$ HNs	10.71	0.747	0.70	5.60

4. Conclusions

In summary, facile solvothermal method has been developed for phase controlled synthesis of SnSe and $SnSe_2$ HNs in oleylamine. The added surfactant 1-DDT plays a key role in controlling the crystal phase of the tin selenides. It is believed that 1-DDT stabilizes Sn^{4+} ions by forming Sn^{4+}-dodecanethiolate complex and produce $SnSe_2$ HNs, whereas in the absence of 1-DDT, Sn^{4+} ions are reduced to Sn^{2+} by oleylamine and SnSe HNs are obtained. The obtained HNs have flower-like morphologies comprised of thin nanosheets of thickness 7-12 nm. When $SnSe_2$ HNs are used as the counter electrode of DSSC, a power conversion efficiency of 5.60% is achieved, which is comparable to that of conventional Pt counter electrode (5.74%). These results showed that SnSe and $SnSe_2$ HNs are promising candidates to replace the precious Pt metal as an efficient electrocatalyst in DSSCs.

Acknowledgements

This work was supported by the Priority Research Center Program (2013-055999) and Basic Science Research Program (2012R1A1A2043731) through the National Research Foundation of Korea (NRF).

Notes and References

Department of Chemistry and GETRC, Kongju National University, 182, Shinkwon, Kongju, Chungnam, 314-701, Republic of Korea. Phone: +82-41-850-8496; Fax: +82-41-850-8613; E-mail: jkim@kongju.ac.kr

†Electronic supplementary information (ESI) available: XPS, EDS spectra of SnSe and $SnSe_2$ HNs, XRD patterns, SEM images, diffuse reflectance spectra, surface area measurements of SnSe and $SnSe_2$ HNs. SEM images and XRD patterns of SnSe and $SnSe_2$ counter electrodes. See DOI:

1 D. V. Talapin, J.-S. Lee, M. V. Kovalenko and E. V. Shevchenko, *Chem. Rev*., 2009, **110**, 389-458.
2 M.-R. Gao, Y.-F. Xu, J. Jiang and S.-H. Yu, *Chem. Soc. Rev*., 2013, **42**, 2986-3017.
3 S. V. Kershaw, A. S. Susha and A. L. Rogach, *Chem. Soc. Rev*., 2013, **42**, 3033-3087.
4 I. Moreels, Y. Justo, B. De Geyter, K. Haustraete, J. C. Martins and Z. Hens, *ACS Nano*, 2011, **5**, 2004-2012.
5 H. Fu and S.-W. Tsang, *Nanoscale*, 2012, **4**, 2187-2201.
6 G. Xiao, Y. Wang, J. Ning, Y. Wei, B. Liu, W. W. Yu, G. Zou and B. Zou, *RSC Adv*., 2013, **3**, 8104-8130.

7 X. Yu, J. Zhu, Y. Zhang, J. Weng, L. Hu and S. Dai, *Chem. Commun*., 2012, **48**, 3324-3326.

8 C. Zhang, H. Yin, M. Han, Z. Dai, H. Pang, Y. Zheng, Y.-Q. Lan, J. Bao and J. Zhu, *ACS Nano*, 2014, **8**, 3761-3770.

9 M. A. Franzman, C. W. Schlenker, M. E. Thompson and R. L. Brutchey, *J. Am. Chem. Soc*., 2010, **132**, 4060-4061.

10 R. Y. Wang, M. A. Caldwell, R. G. D. Jeyasingh, S. Aloni, R. M. Shelby, H.-S. P. Wong and D. J. Milliron, *J. Appl. Phys*., 2011, **109**, 113506-6.

11 L. Li, Z. Chen, Y. Hu, X. Wang, T. Zhang, W. Chen and Q. Wang, *J. Am. Chem. Soc*., 2013, **135**, 1213-1216.

12 J. Choi, J. Jin, I. G. Jung, J. M. Kim, H. J. Kim and S. U. Son, *Chem. Commun*., 2011, **47**, 5241-5243.

13 I. Lefebvre, M. A. Szymanski, J. Olivier-Fourcade and J. C. Jumas, *Phys. Rev. B*, 1998, **58**, 1896-1906.

14 W. J. Baumgardner, J. J. Choi, Y.-F. Lim and T. Hanrath, *J. Am. Chem. Soc*., 2010, **132**, 9519-9521.

15 S. Liu, X. Guo, M. Li, W.-H. Zhang, X. Liu and C. Li, *Angew. Chem. Int. Ed*., 2011, **50**, 12050-12053.

16 D. D. Vaughn, S.-I. In and R. E. Schaak, *ACS Nano*, 2011, **5**, 8852-8860.

17 Z. Fang, S. Hao, L. Long, H. Fang, T. Qiang and Y. Song, *CrystEngComm*, 2014, **16**, 2404-2410.

18 K. Jang, I.-y. Lee, J. Xu, J. Choi, J. Jin, J. H. Park, H. J. Kim, G.-H. Kim and S. U. Son, *Cryst. Growth Des*., 2012, **12**, 3388-3391.

19 D. D. Vaughn, O. D. Hentz, S. Chen, D. Wang and R. E. Schaak, *Chem. Commun*., 2012, **48**, 5608-5610.

20 Y.-L. Zhou, W.-H. Zhou, M. Li, Y.-F. Du and S.-X. Wu, *J. Phys. Chem. C*, 2011, **115**, 19632-19639.

21 T.-L. Hsieh, H.-W. Chen, C.-W. Kung, C.-C. Wang, R. Vittal and K.-C. Ho, *J. Mater. Chem.*, 2012, **22**, 5550-5559.

22 Z. Tang, Q. Tang, J. Wu, Y. Li, Q. Liu, M. Zheng, Y. Xiao, G. Yue, M. Huang and J. Lin, *RSC Adv.*, 2012, **2**, 5034-5037.

23 G. Yue, J. Wu, Y. Xiao, M. Huang, J. Lin and J.-Y. Lin, *J. Mater. Chem. A*, 2013, **1**, 1495-1501.

24 S. Ito, P. Chen, P. Comte, M. K. Nazeeruddin, P. Liska, P. P´echy and M. Gr¨atzel, *Prog. Photovoltaics*, 2007, **15**, 603-612.

25 X. Chen, Y. Hou, B. Zhang, X. H. Yang and H. G. Yang, *Chem. Commun*., 2013, **49**, 5793-5795.